

# Chapter 19

## Transition Metals in Phase-Change Memory Materials: Impact upon Crystallization

Binay Prasai and D.A. Drabold

**Abstract** We employed plane wave density functional molecular dynamics to simulate the crystallization of  $\text{Ge}_2\text{Sb}_2\text{Te}_5$  materials alloyed with  $\sim 2\%$  transition metals (Cu, Ag, and Au) and studied the resulting structural modifications. Despite having very different chemistry, we show that under many circumstances, transition metals join the crystalline structure essentially substitutionally. Bader charge analysis revealed similar positive atomic charges for Cu and Ag whereas negative charge for Au was observed. The optical contrast is preserved in Ag or Au doped  $\text{Ge}_2\text{Sb}_2\text{Te}_5$ , but not in Cu doped  $\text{Ge}_2\text{Sb}_2\text{Te}_5$ . The estimation of the crystallization time for the transition metal doped  $\text{Ge}_2\text{Sb}_2\text{Te}_5$  showed large variation which were attributed to the presence of different fractions of wrong bonds in the alloys.

### 19.1 Introduction

Phase change memory materials offer a remarkable proving ground for ab-initio simulation since direct simulation of the key process of phase change is possible, as discovered in pioneering work of Hegedus and Elliott [1]. In this paper, we extend this research by investigating the role of transition metal (TM) impurities in the phase change process. Remarkably, we find that moderate concentration of certain TMs (Ag and Au) readily join the octahedral crystalline phase, while Cu does not. We report the atomic trajectories leading to full crystallization in detail. We confirm, as in our earlier report, that Ag enhances the crystallization speed [2].

---

B. Prasai (✉) · D.A. Drabold (✉)  
Department of Physics and Astronomy, Ohio University, Athens, OH 45701, USA  
e-mail: bp249507@ohio.edu

D.A. Drabold  
e-mail: drabold@ohio.edu

## 19.2 Methods

Ab-initio molecular dynamic (AIMD) calculations were performed using the Vienna Ab-initio Simulation Package (VASP) [3] to generate models of  $\text{Ge}_2\text{Sb}_2\text{Te}_5$  (GST) and  $\text{X}_{0.17}\text{Ge}_2\text{Sb}_2\text{Te}_5$  ( $\text{X} = \text{Cu}, \text{Ag}, \text{Au}$ ). Each of the models was created in a cubic supercell with 108 (24 Ge atoms, 24 Sb atoms and 60 Te atoms) host atoms and two dopant atoms.

The models were prepared using the “Melt and Quench” method [4], starting with a random configuration at 3000 K. After annealing the random configuration at 3000 K for 25 ps, each model was cooled to 1200 K in 10 ps and equilibrated for 60 ps in the liquid state at 1200 K. A cooling rate of 12 K/ps was adopted to obtain the amorphous models from the melt at 1200–300 K and followed by equilibration at 300 K for another 50 ps. Each of these models was subsequently annealed at 650 K for up to 450 ps to simulate crystallization. The density chosen,  $6.05 \text{ g/cm}^3$ , for undoped  $\text{Ge}_2\text{Sb}_2\text{Te}_5$  is intermediate between the amorphous and crystalline densities. Due to lack of experimental values, same lattice spacing was chosen for doped  $\text{Ge}_2\text{Sb}_2\text{Te}_5$  with the hope that dopants would take the vacancy sites. The density of each system is shown in Table 19.1, and was fixed during the MD runs, and a time step of 5 ps was used.

To compute ground state properties, the models were fully relaxed to a local minimum energy configuration at zero pressure (allowing the cell shape and volume to vary). The final relaxed densities are illustrated in Table 19.1. Three independent models were generated for each of the structures to check the consistency of the results.

The calculations were implemented with the projector augmented-wave (PAW) [5, 6] method to describe electron-ion interactions. The Perdew-Burke-Ernzerhof (PBE) [6, 7] exchange correlation functional was used throughout. Molecular-dynamics (MD) simulations were performed in a cubic supercell at constant volume for annealing, equilibrating and cooling, whereas, zero pressure conjugate gradient (CG) simulations were performed for relaxation. Both the MD and CG simulations were performed by using only the  $\Gamma$  point to sample the supercell Brillouin zone for computing the total energies and forces.

**Table 19.1** Density (in  $\text{gm cm}^{-3}$ ) chosen in different unrelaxed models. The densities employed are compared to the amorphous and crystalline densities of fully relaxed models

Systems	Unrelaxed	Relaxed	
		Amorphous	Crystalline
$\text{Ge}_2\text{Sb}_2\text{Te}_5$	6.05	5.70	6.12
$\text{Cu-Ge}_2\text{Sb}_2\text{Te}_5$	6.11	5.82	6.20
$\text{Ag-Ge}_2\text{Sb}_2\text{Te}_5$	6.20	5.94	6.21
$\text{Au-Ge}_2\text{Sb}_2\text{Te}_5$	6.24	5.88	6.23

## 19.3 Structural Properties

### 19.3.1 Correlation Functions

There have been a number of reports discussing where a dopant sits in the  $\text{Ge}_2\text{Sb}_2\text{Te}_5$  host network [8]. It is therefore interesting to see how these dopants (Cu, Ag, Au) adapt to the local structure. The atomic structure of our models is studied through a set of pair correlation functions. A pair correlation function is a position distribution function based on the probability of finding atoms at some distance  $\mathbf{r}$  from a central atom. Following [9], we tersely develop the expressions for correlation functions and present this below. A general expression for the pair distribution function [9] is:

$$g(\mathbf{r}) = \frac{1}{\rho^2 V} N(N-1) \langle \delta(\mathbf{r} - \mathbf{r}_{ij}) \rangle \quad (19.1)$$

Here,  $\rho$  and  $V$  are the number density and volume respectively of the model,  $N$  the number of neighboring atoms of the central atom and  $r_{ij}$  is the distance of any atom from the central atom. The symbol  $\langle \dots \rangle$  represents a configuration average. The radial pair correlation function can be obtained as

$$g(r) = \int \frac{d\Omega}{4\pi} g(\mathbf{r}) \quad (19.2)$$

or,

$$g(r) = \frac{1}{\rho^2 V} \sum_{i,i \neq j} \int \int \frac{\sin \theta}{4\pi} d\theta d\phi \frac{1}{r^2 \sin \theta} \delta(r - r_{ij}) \delta(\theta - \theta_{ij}) \delta(\phi - \phi_{ij}) \quad (19.3)$$

or,

$$g(r) = \frac{1}{4\pi \rho^2 V r^2} \sum_{i,i \neq j} \delta(r - r_{ij}) \quad (19.4)$$

The pair correlation functions (PCFs) provide local structural information of essential interest for amorphous materials. The peaks in these functions describe the average distance of neighboring atoms from a central atom. Since amorphous materials do not possess long range order,  $g(r) \rightarrow 1$  as  $r \rightarrow \infty$ . For crystalline structures,  $g(r)$  is a sum of delta functions, with each term coming from a coordination shell.

For systems with more than one species, structural correlations are usually investigated through partial pair correlation functions  $g_{\alpha\beta}(r)$ , which are expressed as

$$\langle n_{\alpha\beta}(r) \rangle \Delta r = 4\pi r^2 \Delta r \rho c_\alpha g_{\alpha\beta}(r) \quad (19.5)$$

where  $n_{\alpha\beta}(r) \Delta r$  is number of particles of species  $\beta$  in a shell between  $r$  and  $r+\Delta r$  around a central atom  $\alpha$ ,  $c_\alpha = N_\alpha/N$  is the concentration of species  $\alpha$ . The total

pair correlation function is then defined as the sum of all partial contributions as

$$g(r) = \sum_{\alpha\beta} c_{\alpha}c_{\beta}g_{\alpha\beta}(r) \quad (19.6)$$

In addition to local bonding, integration of the PCF up to the first minimum provides information on mean coordination numbers. Coordination analysis is particularly interesting in these materials since the coordination changes from six in the crystalline phase (rocksalt structure) to about four in the amorphous phase. It should also be pointed out that the information obtained from the PCF alone may not be sufficient to describe the local structure and hence require introduction of simple three-body distribution functions like bond angle distributions (BADs). BAD would lend insight into the local environment of each impurity atom and the network structure of doped phase change materials.

Since crystalline  $\text{Ge}_2\text{Sb}_2\text{Te}_5$  contains of order 20% vacant octahedral sites, these vacant sites would seem to be an ideal place for the dopant atoms to sit. However, as there is no certain definition of vacancy in the amorphous phase, the local structure of the dopant atoms in the amorphous phase is all the more interesting to investigate. The local structures of the dopants are presented in Fig. 19.1. Figure 19.1a–f represent the local structure of the dopants in the amorphous phase, while the bottom half (Fig. 19.1g–l) depict the crystalline phase. Figure 19.2 presents a set of PPCFs corresponding to different dopant atoms. At a dopant concentration near 2%, there is no major change in pair correlation functions for either amorphous or crystalline phases. As the position of the first maximum in the PPCF reflects the average bond lengths, we were able to estimate the average bond lengths and present them in Table 19.2. We observed no dopant-induced change in Ge–Te and Sb–Te average

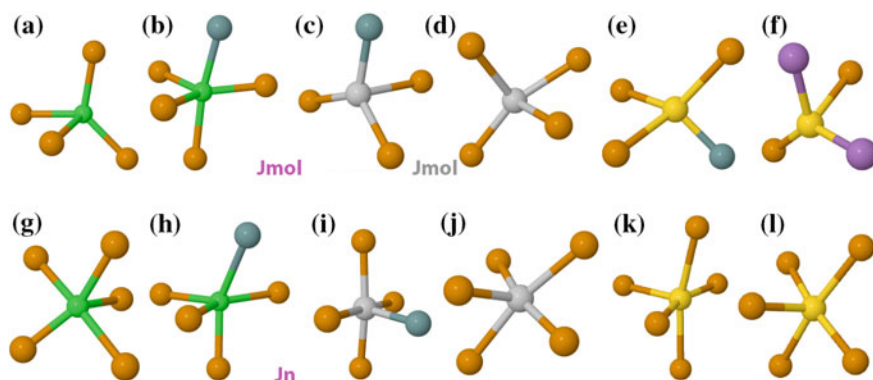


**Fig. 19.1** Local atomic structures surrounding the dopants. **a, b** Cu, **c, d** Ag, and **e, f** Au local geometries in amorphous phases (*top* images). The *bottom* images correspond to structures around the dopants in crystalline phases. Color code: *Orange* Te, *Blue* Ge, *Purple* Sb, *Green* Cu, *Silver* Ag, *Yellow* Au

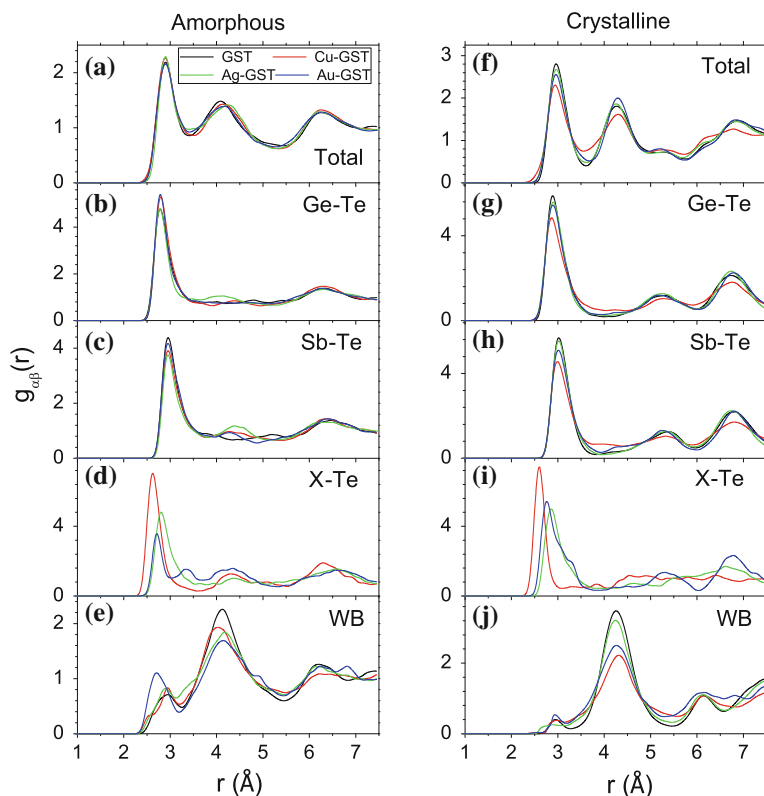
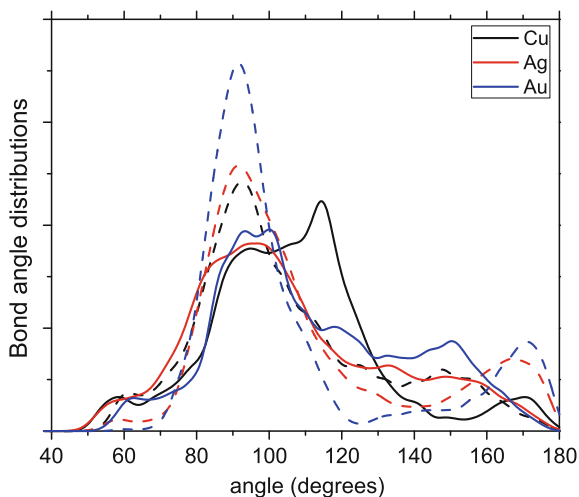


**Fig. 19.2** Pair correlation functions at 300 K for pure and doped  $\text{Ge}_2\text{Sb}_2\text{Te}_5$ . Partial pair correlation functions for amorphous structures are on the left (a–e) and for crystalline structures are on the right (f–j). WB stands for wrong bonds

**Table 19.2** Average bond lengths (Å) in amorphous and crystalline phases of pure and doped  $\text{Ge}_2\text{Sb}_2\text{Te}_5$

Bonds	Dopant	Amorphous	Crystalline
Ge-Te	–	2.78	2.92
	Cu	2.78	2.91
	Ag	2.78	2.92
	Au	2.78	2.92
Sb-Te	–	2.96	3.02
	Cu	2.96	3.00
	Ag	2.96	3.02
	Au	2.96	3.02
Cu-Te	Cu	2.59	2.62
Ag-Te	Ag	2.82	2.88
Au-Te	Au	2.72	2.78

**Fig. 19.3** Bond angle distributions around the dopants at 300 K for doped  $\text{Ge}_2\text{Sb}_2\text{Te}_5$ . Dashed lines are bond angle distributions for crystalline  $\text{Ge}_2\text{Sb}_2\text{Te}_5$



bond lengths in the amorphous phase, whereas the change in Ge–Te and Sb–Te average bond lengths in crystalline phase is also negligible being within the uncertainty of  $\sim 0.01 \text{ \AA}$ . On the other hand, the Cu–Te average bond length is observed to be the shortest while Ag–Te average bond length is the longest among the three dopants. To further detail the local topology of the dopants, we computed the bond angle distribution (BAD) centered on the dopants and illustrate the results in Fig. 19.3, which reveals a substantial distortion of the BADs in the amorphous phase while the BADs in the crystalline phase illustrate the remarkable tendency of the dopants to adopt an octahedral geometry, just as the host atoms. Among the three dopants, Cu is least likely to adopt octahedral geometry as compared to Ag and Au since no peak at around  $180^\circ$  is observed for Cu BAD. The reason could be the shorter Cu–Te bond lengths as compared to Ag–Te and Au–Te bond lengths or the wide variation of acceptable valency of Cu.

To investigate the dopant impact on coordination, we computed coordination numbers by integrating the PPCFs up to the first minimum in the RDF, and present results in Table 19.3. Among the three dopants, Cu has the highest coordination number. Furthermore, the coordination number of Cu does not change significantly from the amorphous to crystalline phase. Beside this, the coordination numbers of the host species (Ge/Sb/Te) do not change significantly as in pure GST or doped with Ag or Au, suggesting that the presence of Cu in the GST might suppress the phase transition, thereby reducing the crystallization speed. Au on the other hand, tends to exhibit a significant fraction of Ge/Sb atoms as neighbors although Te is the most anionic species (no Ge/Sb neighbors are observed in the crystalline phase). Unlike Cu, the coordination numbers of Au as well as the host species in Au-doped GST increase significantly. Ag also shows some Ag–Ge and Ag–Sb ( $< 10\%$ ) bonds, which persist even to the crystalline phase of Ag-doped GST however, Ag does not suppress the increase in the coordination numbers like Cu.

**Table 19.3** Comparison of coordination numbers in amorphous and crystalline phases of pure and doped  $\text{Ge}_2\text{Sb}_2\text{Te}_5$ . A cutoff distance of 3.2 Å was chosen for integration of the first peak of PPCF

Species	Dopant	Amorphous					Crystalline				
		Ge	Sb	Te	X	Total	Ge	Sb	Te	X	Total
Ge	–	0.4	0.3	3.5	–	4.2	–	0.1	5.4	–	5.5
	Cu	0.2	0.3	3.8	–	4.3	–	0.1	4.6	–	4.7
	Ag	0.1	0.5	3.2	–	3.8	0.1	0.2	5.1	–	5.4
	Au	0.4	0.2	3.6	–	4.2	0.1	–	5.0	–	5.1
Sb	–	0.3	0.5	2.8	–	3.6	0.1	0.3	5.2	–	5.6
	Cu	0.3	0.7	2.7	–	3.7	0.1	0.5	4.2	–	4.8
	Ag	0.5	0.6	2.6	–	3.7	0.2	0.1	4.9	–	5.2
	Au	0.2	0.5	2.9	0.1	3.7	–	0.3	4.7	–	5.0
Te	–	1.4	1.1	0.2	–	2.7	2.2	2.1	0.2	–	4.5
	Cu	1.5	1.1	0.4	0.1	3.1	1.8	1.7	0.2	0.1	3.8
	Ag	1.3	1.0	0.4	0.1	2.8	2.0	2.0	0.2	0.2	4.4
	Au	1.5	1.1	0.3	0.1	3.0	1.8	1.7	0.2	0.1	3.8
Cu	Cu	0.6	–	4.2	–	4.8	0.5	–	4.5	–	5.0
Ag	Ag	0.3	0.1	3.5	–	3.9	0.3	0.2	4.5	–	5.0
Au	Au	0.5	1.0	1.9	–	3.4	–	–	5.2	–	5.2

**Table 19.4** Computed average atomic charges on the dopant atoms in relaxed amorphous and crystalline phases of Cu, Ag, and Au doped  $\text{Ge}_2\text{Sb}_2\text{Te}_5$ . The charges are in the unit of e

Dopants	Amorphous	Crystalline	Change (%)
Cu	0.16	0.12	25
Ag	0.14	0.08	43
Au	–0.44	–0.28	36

Coordination analysis reveals that the majority of the dopant atoms bond to Te rather than Ge and Sb (see Table 19.3). Cu, Ag, and Au have 88, 90, and 56% Te nearest neighbors, respectively. Au seems noticeably different than Cu or Ag with only 56% Te as first neighbor. This contrast is interesting, since the three elements lie on the same column of the periodic table and might be supposed to have similar coordination. To further explore the coordination, we computed the average atomic charge on the dopant atoms using a Bader analysis [10–12] and present the results in Table 19.4. We observe similar atomic charges for Cu and Ag whereas we obtain a negative charge for Au. The negative charge on Au makes it anionic, and a consequence is that a large fraction of Ge and Sb are bonded to Au. The atomic charge on Au becomes significantly less negative in the crystalline phase and the fraction of Ge and Sb neighbors drops.

Beside Ge–Te, Sb–Te and X–Te (X = Cu, Ag, and Au) bonds, there are a number of other bond pairs such as, Ge–Sb, Ge–X, and Sb–X bonds which are often termed

“wrong bonds” (Fig. 19.2e, j). About 14% of the total bond pairs are wrong bonds (WB) in the amorphous phase, whereas about 5% of wrong bonds persist in the crystalline phase.

## 19.4 Electronic and Optical Properties

Practical utilization of GST materials depends upon a substantial optical or electrical contrast between the amorphous and crystalline phases. As both the resistivity and optical absorption depend upon the electronic structures of materials, it is necessary to investigate the influence of dopants on the electronic structure of the host network.

The electronic structure is described by the electronic density of states (EDOS), projected density of states (PDOS), and inverse participation ratio (IPR) of each individual state. The EDOS is defined as:

$$g(E) = \frac{1}{N_b} \sum_{i=1} \delta(E - E_i), \quad (19.7)$$

in which  $N_b$  is the number of basis orbitals, and in this work,  $E_i$  are Kohn-Sham eigenvalues. The EDOS provides information about the electronic gaps, the PDOS provides information on the defects or irregularities in the topology. A common expression for PDOS is:

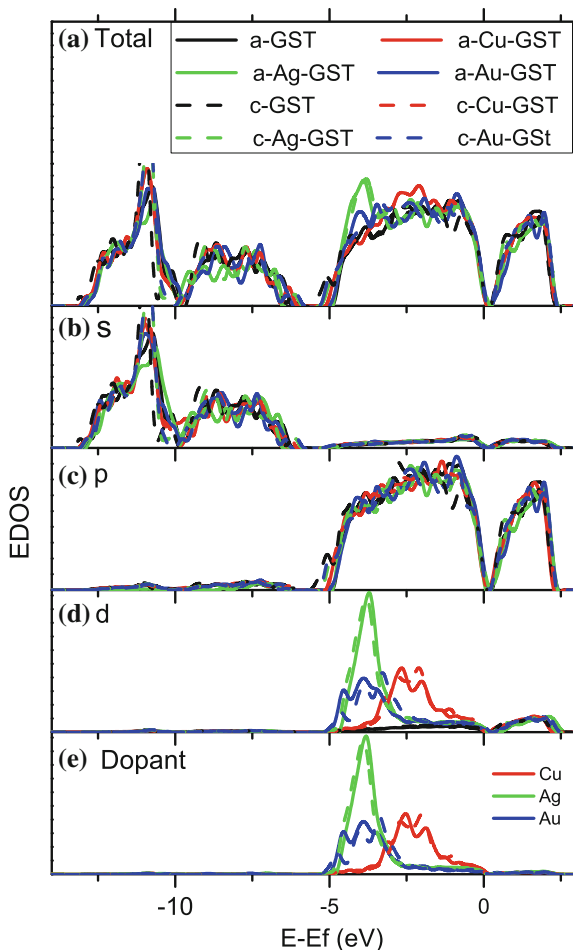
$$g_n(E) = \frac{1}{N_b} \sum_{i=1} \delta(E - E_i) |\langle \phi_n | \Psi_i \rangle|^2 \quad (19.8)$$

where  $g_n(E)$  is site projected DOS for the site  $n$ ,  $\phi_n$  is the local orbital and  $\Psi_i$  is the  $i$ th Kohn-Sham eigenvector.

To investigate the effect of dopants on the electronic properties we computed both the species-projected and orbital-projected (PDOS) and present these in Fig. 19.4a–e. At  $\sim 2\%$  dopant level, we were not able to observe a significant difference in the total density of states except for slight variation in the energy range of  $-5$  to  $-1$  eV below the Fermi level. This change mainly corresponds to the d states of the dopants (Fig. 19.4d, e). Among the dopants, Cu d states lie closer to the band gap and therefore the presence of Cu may significantly affect the electrical and optical properties. This is presumably the ultimate origin of the difference in the local topology of Cu impurities. Of course, the present calculations underestimate the experimental band gaps as expected for DFT [13].

To observe the influence of dopants on the optical properties of  $\text{Ge}_2\text{Sb}_2\text{Te}_5$ , we computed the dielectric functions of the pure and doped  $\text{Ge}_2\text{Sb}_2\text{Te}_5$ . Figure 19.5 presents the imaginary and real part of the dielectric functions of pure and doped  $\text{Ge}_2\text{Sb}_2\text{Te}_5$  in both the amorphous and the crystalline phases. Figure 19.5 confirms that the addition of Ag or Au does not affect the optical properties strongly,

**Fig. 19.4** Comparison of partial density of states (PDOS) for different dopants in  $\text{Ge}_2\text{Sb}_2\text{Te}_5$ . The Fermi level is set to 0 eV



preserving the optical contrast in the visible regions (1–3 eV) whereas the addition of Cu does not look promising in terms of optical contrast. Table 19.5 presents the optical dielectric constant, i.e., the lower energy-limit of the real part of the dielectric function ( $\omega \rightarrow 0$ ). The reduction in optical contrast on adding Cu can be attributed the structure of Cu in the host network. We observe almost no change in the Cu–Te bond lengths as well as the Cu coordination numbers during the phase transition suggesting Cu very immobile in the host network. As discussed by Shportko et al. [14], the contrast in the optical properties in PCMM is attributed to a large electronic polarizability in the crystalline phase due to resonant (electron deficient) p-bonding. Unlike Ag and Au, Cu is unable to integrate itself fully into the crystalline structure with octahedral structure (see Fig. 19.1) introducing a significant structural disorder and hence reducing the contribution to the resonant bonding. This reduction would cause the decrease in the optical contrast.

**Fig. 19.5** Comparison of optical contrast in Cu, Ag, and Au doped  $\text{Ge}_2\text{Sb}_2\text{Te}_5$

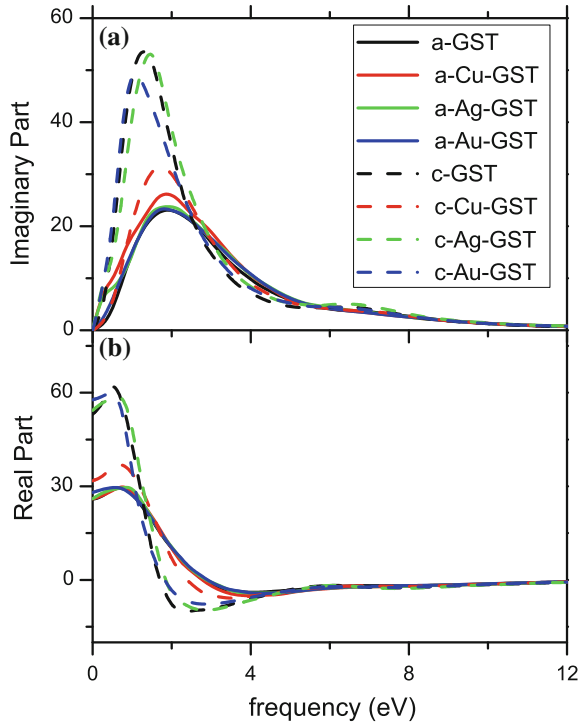


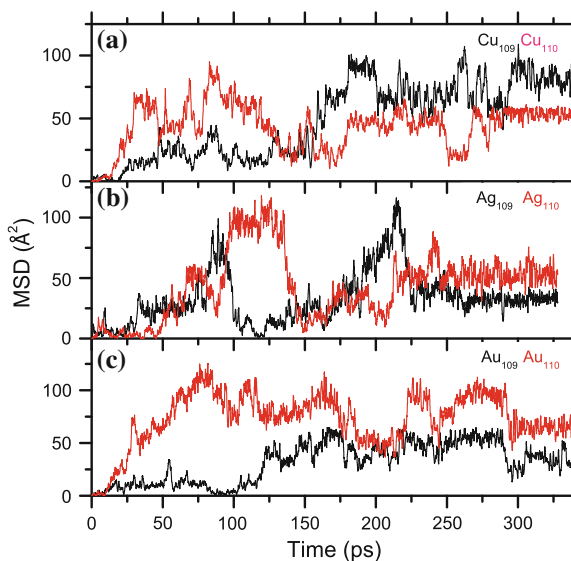
**Table 19.5** Comparison of the optical dielectric constant between the two phases of pure and doped  $\text{Ge}_2\text{Sb}_2\text{Te}_5$

Dopants	Amorphous	Crystalline	Increase (%)
–	25.9	53.0	105
Cu	26.0	31.7	22
Ag	26.1	54.3	108
Au	28.1	57.7	105

### 19.5 Crystallization Dynamics

The dopant centered bond angle distributions (Fig. 19.3) illustrate the modification of local geometry of dopants from wide distortion to more ordered octahedral structures. This makes it possible to observe the atomic motion of dopants during and after the crystallization of the host network is completed. There have been few studies on the dynamics of dopants in  $\text{Ge}_2\text{Sb}_2\text{Te}_5$  during crystallization [8, 15]. In the simulations with the first row dopants (Sc-Zn), Skelton and Elliott have reported a range of atomic motion even after crystallization [8]; however only one dopant was investigated. In their recent work, Prasai et al. investigated the dynamics of Ag in  $\text{Ge}_2\text{Sb}_2\text{Te}_5$  with up to 12% Ag, and reported mixed diffusion of Ag. We observe atomic motion during and after crystallization of host network in the present work as presented in Fig. 19.6. A thorough investigation of atomic diffusion reveals that the dopant atoms

**Fig. 19.6** Mean squared displacements (MSD) of dopants during the crystallization process



become less diffusive whenever the atom is close to octahedral geometry. Figure 19.6 shows the mean-squared displacement of each of the dopant atoms through the entire crystallization process. Both Ag or Au atoms show no hopping after crystallization, whereas a particular Cu atom, Cu<sub>109</sub> shows hopping even after the crystallization has occurred. The local geometries of the dopant atoms are shown in the Fig. 19.1a–l. The dopant atom that achieve octahedral geometry exhibit no hopping after the crystallization. Cu<sub>109</sub> (one of two Cu atoms) showed hopping after the crystallization, and did not achieve the octahedral geometry over the time of the simulation. Cu<sub>109</sub> is represented by Fig. 19.1a, g in amorphous and crystalline phases respectively.

We also analyze the average atomic charge on the dopants during the crystallization of Ge<sub>2</sub>Sb<sub>2</sub>Te<sub>5</sub>. Figure 19.7 presents the time evolution of the average atomic charge on Au along with the nearest neighbors of Au within the first coordination shell. The fraction of Ge/Sb neighbors decreases while increasing the fraction of Te neighbors as the charge on Au decreases.

The speed of crystallization was investigated by observing the time evolution of the total energy of the system (Fig. 19.8). Each of the models was annealed at 650 K until crystallized. Based on the evolution of energy, the total crystallization process can be divided into three regions as also explained by Lee et al. [16]. During Period I (incubation period), although the total energy does not change significantly, the number of four-fold (square) rings kept increasing forming cubes or planes with random orientations driven by thermal fluctuations [2, 16]. Period II, in which the total energy shows a monotonous decrease, is the time in which the cubes or planes start arranging themselves into more globally ordered structures. By the end of this

**Fig. 19.7** Evolution of the average charge on Au during crystallization of Au-doped  $\text{Ge}_2\text{Sb}_2\text{Te}_5$ . The number of nearest neighbors in the first coordination shell is presented for comparison. Only Au charge evolution is presented for comparison purpose

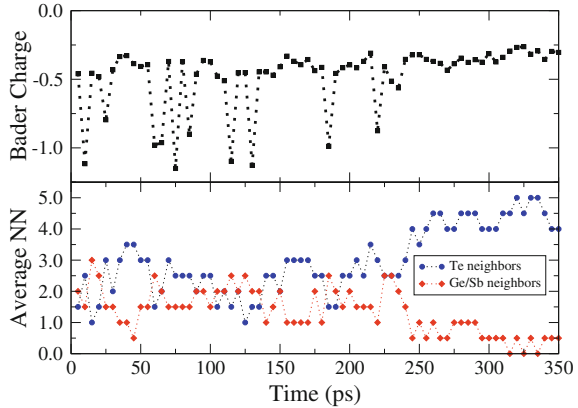
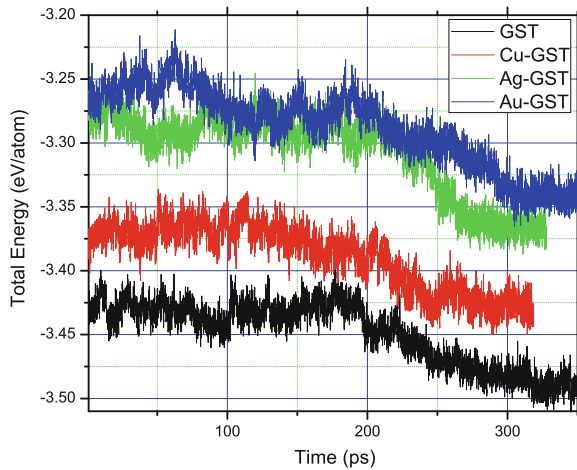


**Fig. 19.8** Evolution of total energy in pure and doped  $\text{Ge}_2\text{Sb}_2\text{Te}_5$  annealed at 650 K. The drop in the total energy represents the crystallization



period the energy goes to a minimum and remains more or less constant thereafter reaching Period III where the crystallization is complete. The duration of Periods I and II shows large fluctuation for three independent models for same structure resulting in significant uncertainty for estimation of crystallization time. These fluctuations are mainly associated with the fraction of wrong bonds present in the amorphous phase as well as the random orientations of the square rings due to thermal fluctuations. Table 19.6 presents the average fraction of wrong bonds and the crystallization time from three different models of varying composition. Although the crystallization periods show large variation, the time of about 400 ps was enough for each of the models to complete crystallization. While we may not be able to predict the exact modification on the crystallization speed at this level but it is confirmed that the crystallization speed of the host network is preserved.

**Table 19.6** Computation of wrong bonds and the estimation of the crystallization time in doped and undoped  $\text{Ge}_2\text{Sb}_2\text{Te}_5$ 

Dopant	Wrong bonds in fraction	Incubation period (ps)	Crystallization period (ps)	Total (ps)
–	$0.13 \pm 0.03$	$150 \pm 50$	$120 \pm 40$	$270 \pm 90$
Cu	$0.14 \pm 0.03$	$180 \pm 30$	$120 \pm 45$	$300 \pm 75$
Ag	$0.15 \pm 0.04$	$130 \pm 40$	$100 \pm 20$	$230 \pm 60$
Au	$0.14 \pm 0.04$	$170 \pm 50$	$120 \pm 30$	$290 \pm 80$

## 19.6 Conclusion

The phase change memory materials present an opportunity unique in materials theory: a chemically complex system of huge technical importance, and a rapidity of phase transformations that enables the direct simulation with the most accurate methods.

We used ab initio molecular dynamic simulations to study crystallization of Ge–Sb–Te phase change alloys in the presence of transition metals (Cu, Ag, and Au) impurities. We were able to simulate the ultrafast phase transitions from amorphous to crystalline phase through the MD simulations. At  $\sim 2\%$  of impurities, we did not observe any significant dopant-induced structural change in Ge–Te or Sb–Te average bond lengths. Meanwhile the Bader charge analysis confirmed similar positive charge for Cu and Ag whereas negative charge for Au as a consequence Au was observed to have significant amount of Ge/Sb as neighbors. The estimation of dielectric constant in amorphous and crystalline phase implies that the optical contrast is preserved in Ag or Au doped  $\text{Ge}_2\text{Sb}_2\text{Te}_5$  while Cu doped  $\text{Ge}_2\text{Sb}_2\text{Te}_5$  did not look too promising in terms of optical contrast. We were also able to estimate the crystallization time for the transition metal doped  $\text{Ge}_2\text{Sb}_2\text{Te}_5$  however with large variations which may be attributed to the presence of WB in the system.

**Acknowledgments** The authors would like to thank Professor S. R. Elliott for many helpful suggestions. This work was supported by the Army Research Office under Grant No W911NF1110358. This work was also supported in part by an allocation of computing time from the Ohio Supercomputer Center.

## References

1. J. Hegedus, S.R. Elliott, Microscopic origin of the fast crystallization ability of Ge–Sb–Te phase-change memory materials. *Nat. Mater* **7**, 399–405 (2008)
2. B. Prasai, G. Chen, D.A. Drabold, Direct ab-initio molecular dynamic study of ultrafast phase change in Ag-alloyed  $\text{Ge}_2\text{Sb}_2\text{Te}_5$ . *Appl. Phys. Lett.* **102** (2013)
3. G. Kresse, J. Furthmüller, Efficiency of ab-initio total energy calculations for metals and semiconductors using a plane-wave basis set. *Comput. Mater. Sci.* **6**(1), 15–50 (1996)
4. D.A. Drabold, Topics in the theory of amorphous materials. *Eur. Phys. J. B* **68**, 1–21 (2009)
5. P.E. Blöchl, Projector augmented-wave method. *Phys. Rev. B* **50**, 17953–17979 (1994)
6. G. Kresse, D. Joubert, From ultrasoft pseudopotentials to the projector augmented-wave method. *Phys. Rev. B* **59**, 1758–1775 (1999)

7. J.P. Perdew, K. Burke, M. Ernzerhof, Generalized gradient approximation made simple. *Phys. Rev. Lett.* **77**, 3865–3868 (1996)
8. J.M. Skelton, S.R. Elliott, In silico optimisation of phase-change materials for digital memories: a survey of first-row transition-metal dopants for  $\text{Ge}_2\text{Sb}_2\text{Te}_5$ . *J. Phys. Condens. Matter* **25**, 205801 (2013)
9. N.E. Cusack, in *The Physics of Structurally Disordered Matter: An Introduction*, ed. by D.F. Brewer, D. Phil, pp. 30–36 (1987)
10. W. Tang, E. Sanville, G. Henkelman, A grid-based bader analysis algorithm without lattice bias. *J. Phys. Condens. Matter* **21**, 084204 (2009)
11. E. Sanville, S.D. Kenny, R. Smith, G. Henkelman, An improved grid-based algorithm for bader charge allocation. *J. Comp. Chem.* **28**, 899–908 (2007)
12. G. Henkelman, A. Arnaldsson, H. Jonsson, A fast and robust algorithm for bader decomposition of charge density. *Comput. Mater. Sci.* **36**, 254–360 (2006)
13. A. Seidl, A. Gorling, P. Vogl, J.A. Majewski, M. Levy, Generalized kohn-sham schemes and the band-gap problem. *Phy. Rev. B.* **53**, 3764–74 (1996)
14. K. Shportko, S. Kremers, M. Woda, D. Lencer, J. Robertson, M. Wuttig, Resonant bonding in crystalline phase-change materials. *Nat. Mater.* **7**, 653–658 (2008)
15. B. Prasai, M.E. Kordesch, D.A. Drabold, G. Chen, Atomistic origin of rapid crystallization of Ag-doped Ge-Sb-Te alloys: a joint experimental and theoretical study. *Physica Status Solidi B* **102**, 1–6 (2013)
16. T.H. Lee, S.R. Elliott, Ab-Initio computer simulation of the early stages of crystallization: application to  $\text{Ge}_2\text{Sb}_2\text{Te}_5$  phase-change materials. *Phys. Rev. Lett.* **107**, 145702 (2011)